Microsystem Technologies
https://doi.org/10.1007/s00542-022-05405-6

TECHNICAL PAPER

Fabrication process for FEP piezoelectrets based on photolithographically structured thermoforming templates

D. Flachs[1] · F. Emmerich[1] · C. Thielemann[1]

Received: 27 September 2021 / Accepted: 23 November 2022

Abstract
Piezoelectrets fabricated from fluoroethylenepropylene (FEP)-foils have shown drastic increase of their piezoelectric properties during the last decade. This led to the development of FEP-based energy harvesters, which are about to evolve into a technology with a power-generation-capacity of milliwatt per square-centimeter at their resonance frequency. Recent studies focus on piezoelectrets with solely negative charges, as they have a better charge stability and a better suitability for implementation in rising technologies, like the internet of things (IOT) or portable electronics. With these developments heading towards applications of piezoelectrets in the near future, there is an urgent need to also address the fabrication process in terms of scalability, reproducibility and miniaturization. In this study, we firstly present a comprehensive review of the literature for a deep insight into the research that has been done in the field of FEP-based piezoelectrets. For the first time, we propose the employment of microsystem-technology and present a process for the fabrication of thermoformed FEP piezoelectrets based on thermoforming SU-8 templates. Following this process, unipolar piezoelectrets were fabricated with air void dimensions in the range of 300–1000 µm in width and approx. 90 µm in height. For samples with a void size of 1000 µm, a d_{33}-coefficient up to 26,508 pC/N has been achieved, depending on the applied seismic mass. Finally, the properties as energy harvester were characterized. At the best, an electrical power output of 0.51 mW was achieved for an acceleration of 1 × g with a seismic mass of 101 g. Such piezoelectrets with highly defined dimensions show good energy output in relation to volume, with high potential for widespread applications.

1 Introduction

Piezoelectrets are dielectric polymers with an internal air void structure, showing piezoelectric properties after the material has been electrically charged. If mechanical stress is applied, piezoelectrets provide an externally measurable voltage. Depending on the manufacturing process, the inner cavities of the piezoelectrets may be geometrically controlled, which provides some degree of freedom in the piezoelectric properties.

Over the last decade, the performance of fluorocarbon-based piezoelectrets, with respect to their piezoelectric coefficient, have shown a tremendous increase with values of up to several thousand pC/N (Zhang et al. 2014) (Emmerich and Thielemann 2018; Zhang et al. 2015, 2013, 2012). These piezoelectrets are usually based on polytetrafluoroethylene (PTFE) or fluoroethylene-propylene (FEP). Especially the latter encouraged the development of FEP-based vibration-energy-harvesters, which are emerging in the mW/cm^2 range (Zhang et al. 2018). These values—after further improvement—promise future applications of these harvesters in mobile consumer electronics. Another striking argument for polymer-based piezoelectrets is that major drawbacks known for classic piezoelectric ceramics, such as difficult processing and brittleness, are no issue. With the goal to increase the generated energy and usability, various studies address the production process and the performance of these piezo-electret-based harvesters. For different designs, they show

D. Flachs and F. Emmerich have contributed equally to this work.

✉ D. Flachs
dennis.flachs@th-ab.de

F. Emmerich
biomems@th-ab.de

C. Thielemann
christiane.thielemann@th-ab.de

[1] Biomems lab, Technische Hochschule Aschaffenburg, Würzburger Straße 45, 63743 Aschaffenburg, Germany

Published online: 12 December 2022

promising results in d_{33}-mode (Zhang et al. 2015) as well as in d_{31}-mode (charge generated perpendicular to direction of pressure) (Zhang et al. 2016a). Piezoelectrets store, after charging, a quasi-permanent electric charge with a slow decay in the range of months and years. As many piezoelectrets are based on a bipolar charge distribution with a not negligible charge decay of positive charges over longer time periods, additional approaches suggest the use of an unipolar negative charge setup, to improve the long-term charge stability. The energy conversion of energy harvesters based on unipolar piezoelectrets is due to a wavy electret film and two electrodes, using the principle of a gap closing variable capacitor, where the electret film is used to assume the role of a constant bias voltage (active device) (Zhang et al. 2018).

In the first part of this paper, we present a comprehensive overview of the state-of-the-art in the field of FEP-based piezoelectrets. In the second part, we introduce a new approach to fabricate FEP piezoelectrets based on photolithographically structured SU-8 thermoforming templates. A detailed analysis of the resulting structure shapes is conducted and finally, charge sensitivity in unipolar piezoelectrets is measured for different air void geometries and used for calculations of the output power in energy-harvesting applications.

2 State-of-the-art of FEP-based piezoelectrets

A standard fabrication process for piezoelectrets is the foaming of polypropylene (PP)-foil to achieve non-uniform micron-sized air voids inside the material (Lekkala et al. 1996). After foaming, the material is charged by a high voltage corona set-up or a high-voltage DC-source. During charging, the electric field strength inside the air voids exceeds the breakdown strength of the embedded air, causing a dielectric barrier discharge (DBD). This procedure results in charging of both void surfaces with opposite polarity, see Fig. 1a. Alternatively—to improve the long-term charge stability—unipolar charge schemes are also common and therefore have been addressed in this work.

More temperature stable materials, like FEP, provide better charge stability than PP. However, foaming of FEP is difficult resulting in significantly lower d_{33}-coefficients. Thus, more sophisticated approaches were developed for the fabrication of FEP piezoelectrets with tunnel structures and tailored void sizes. A schematic cross section of bipolar and unipolar FEP piezoelectrets with the most important geometric parameters is given in Fig. 1a and b with:

- w_a: width of active (charged) area
- w_p: width of passive (uncharged) area
- s_1: thickness of FEP-layer
- s_2: maximum thickness of the air void
- s_{tot}: maximum thickness of the piezoelectret

Different studies seized this approach and modified the process. A general workflow for the making of FEP-based piezoelectrets is described with the following three steps: (1) the preparation of a thermoforming template, (2) the thermoforming of one or more foils of FEP, and (3) the assembly. While the fabrication process of the thermoforming template determines the geometry of the air voids, the thermoforming-process controls the dimensional accuracy of the formed structure. During assembly, which involves fusion-bonding, metallization and charging of the FEP-foils, the choice of methods and materials strongly influences the longevity of the piezoelectret. The general process is depicted in Fig. 2.

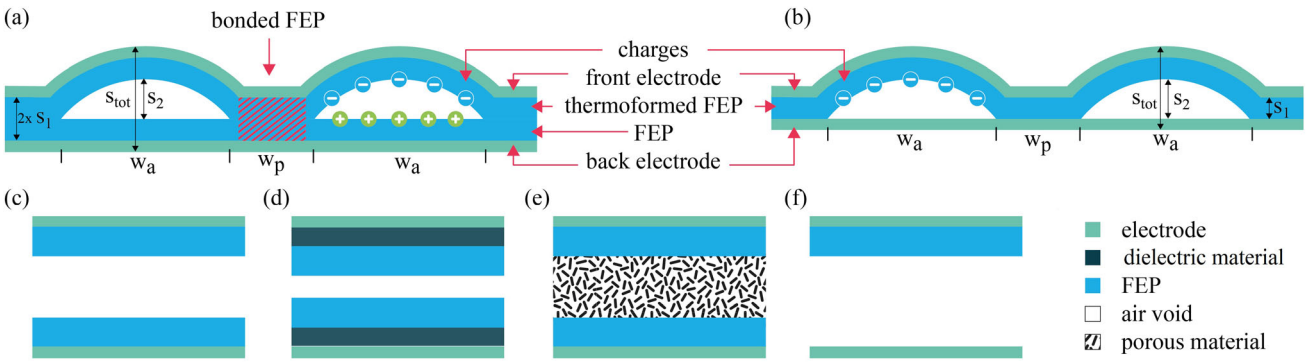

Fig. 1 Schematics for FEP-based piezoelectrets in different levels of complexity. Cross-section schematics for **a** bipolar as well as **b** unipolar FEP piezoelectrets are depicted with the most important geometric values. In **c**–**f** a simplified layer schematic of different piezoelectret types is presented for the categorization in Table 1. **c** shows bipolar piezoelectrets with air void and a single layer electret, **d** bipolar piezoelectrets with air void and a multi-layer electret, **e** bipolar piezoelectrets without air void and porous material and **f** unipolar piezoelectrets with air void and a single layer electret

Table 1 Survey of publications concerning FEP-based piezoelectrets in agreement with Fig. 1

Author	Type	FEP-thickness in µm	Lateral dimensions in µm	Vertical dimensions in µm	Quasistatic d_{33}-coeff. in pC/N	Y in MPa	Comment
This work	(f)	s_1: 12.5	w_a: 300–1000 w_p: 150–500	s_{tot}: 102.5 s_2: 90	–	–	Dyn. d_{33}-coefficient of 26,508 pC/N (resonance)
Ma et al. (2021)	(f)	s_1: 12.5	w_a: 200 w_p: 100	s_{tot}: 160 s_2: 147.5	–	460	Effektive piezoeletric coefficient of 653 nC/N
Zuo et al. (2020)	(c)	s_1: 12.5	w_a: 1500 w_p: 500	s_{tot}: 525 s_2: 500	5300	–	Dyn. d_{33}-coefficient of 40,000 pC/N (resonance)
Zhukov et al. (2020)	(c)	s_1: 25 & 50	w_a: 1300	s_{tot}: 400 s_2: 350	290	–	Single tube
Ma et al. (2019)	(c)	s_1: 12.5	w_a: 1.000 w_p: 500	s_{tot}: 160 s_2: 147.5	–	3	Effective piezoelectric coefficient of41.8 nC/N
Emmerich and Thielemann (2018)	(f)	s_1: 12.5	w_a: 1,000 w_p: 500	s_{tot}: 75 s_2: 50	1850	–	
Zhukov et al. (2017)	(c)	s_1: 50 & 120	w_a: 1250 w_p: 120	s_{tot}: 500 s_2: 400	160	0.3	Produced from tubes
Nepal et al. (2017)	(c)	s_1: 50	w_a: 1500 w_p: 1500	s_{tot}: 150–400 s_2: 50-300	–	–	Examination of charging behavior
Zhang et al. (2016)	(c) (e)	s_1: 12.5	w_a: 1000 w_p: 500	s_{tot}: 82.5 s_2: 45	307	0.25	Porous PTFE acts as spring
Zhang et al. (2016a)	(c)	s_1: 12.5	w_a: 1000 w_p: 500	s_{tot}: 350 s_2: 325	–	–	Application as Energy-Harvester in d_{31}-Mode
Qiu and Gerhard (2016)	(c)	s_1: 50	w_a: 1500 w_p: 1500	s_{tot}: 200 s_2: 100	73	–	Examination of different gases
Rychkov et al. (2015)	(f)	s_1: 50	w_a: 1500 w_p: 1500	s_{tot}: 165 s_2: 80	140	–	Aluminum-foil as back-electrode
Hillenbrand et al. (2015)	(c)	s_1: 25	–	s_{tot}: 35–75 s_2: 10–50	–	–	Smaller air voids have higher output power
Assagra et al. (2015)	(c)	s_1: 50	w_a: 2000 w_p: 2000	s_{tot}: 400 s_2: 300	550	–	Alternative process with embedded water
Araújo et al. (2015)	(c)	s_1: 50	w_a: 1500 w_p: 1500	s_{tot}: 200 s_2: 100	–	–	Application as pressure sensor
Zhang et al. (2015)	(c)	s_1: 12.5	w_a: 500 w_p: 250 w_a: 1000 w_p: 500	s_{tot}: 60–500 s_2: 35–475	3300	0.2–0.5	Application as Energy-Harvester in d_{33}-Mode
Wang et al. (2015)	(c)	s_1: 12.5	w_a: 500 w_p: 250 w_a: 1000 w_p: 500	s_{tot}: 290 s_{tot}: 279	1000	0.32 0.21	Cross-tunnel structure
Zhang et al. (2014)	(c)	s_1: 12.5	w_a: 1000 w_p: 500 w_a: 500 w_p: 250	s_{tot}: 60–500 s_2: 35–475	3700	0.1–0.5	Cross-tunnel structure
Rychkov et al. (2014)	(f)	s_1: 50	w_a: 1500 w_p: 1500	s_{tot}: 215 s_2: 130	57	–	Aluminum-foil as back-electrode
Zhang et al. (2012)	(c)	s_1: 12.5	w_a: 1000 (round)	s_{tot}: 85–190 s_2: 60–165	1000–3000	0.21	Best results for thinnest sample
Wirges et al. (2012)	(c)	s_1: 25	w_a: 1500 w_p: 1500	s_{tot}: 100 s_2: 50	494	0.32	
Medeiros et al. (2012)	(e)	s_1: 50	w_a: 1500 w_p: 1,500	s_{tot}: 200 s_2: 100	–	–	Application as Hydro-phone

Table 1 (continued)

Author	Type	FEP-thickness in µm	Lateral dimensions in µm	Vertical dimensions in µm	Quasistatic d_{33}-coeff. in pC/N	Y in MPa	Comment
Lou et al. (2012)	(e)	s_1: 12.5	w_a: 500 w_p: 400 w_a: 500 w_p: 200	s_{tot}: 48-60 s_2: 23–35	150–360	0.48–1.07	Porous layer acting as spring
Fang et al. (2012)	(c)	s_1: 50	w_a: 3.000 w_p: 1,000	s_{tot}: 150 s_2: 50	280	0.3	Laser-bonding
Altafim et al. (2012)	(c)	s_1: 50	w_a: 1500 w_p: 1500	s_{tot}: 200 s_2: 100	350	1.4	Examined also LDPE
Altafim et al. (2012)	(c)	s_1: 50	w_a: 1400–2500 w_p: 1500–2000	s_{tot}: 125–200 s_2: 25–100	200–485	–	Smaller air voids have higher d_{33}-coefficients
Sun et al. (2011)*	(e)	s_1: 12.5	w_a: 1000 w_p: 200	s_{tot}: 47.5 s_2: 22.5	300	0.28	Porous layer acting as spring
Sun et al. (2011)	(e)	s_1: 12.5	w_a: 1000 w_p: 200	s_{tot}: 47.5 s_2: 22.5	300	0.37	Porous layer acting as spring
Gerard et al. (2011)	(d)	s_1: 50	w_a: 1200 (round)	s_{tot}: 325–1250 s_2: 100–500	–	–	Difficult production process
Falconi et al. (2011)	(c)	s_1: 50	w_a: 3500 (round)	s_{tot}: 400 s_2: 225	70	–	Gluing instead of bonding
Cao et al. (2011)	(c)	s_1: 12.5	w_a: 1,000 w_p: 500	s_{tot}: 80 s_2: 45	220	0.48	Multilayer with porous layer acting as spring
Altafim et al. (2011)	(c)	s_1: 50	w_a: 1500 w_p: 1500	s_{tot}: 200 s_2: 100	275	2.5	Difference between open and closed channels
Altafim et al. (2011)	(c)	s_1: 50	w_a: 1500 w_p: 1500	s_{tot}: 200–500 s_2: 100–300	80-120	3.6-6.3	Multiple cavities on top of each other
Zhang et al. (2010)	(c)	s_1: 12.5	w_a: 1000 w_p: 500	s_{tot}: 47.5 s_2: 22.5	500	0.49–0.76	Multilayer system, more layers have higher Y
Altafim et al. (2010)	(c)	s_1: 50	w_a: 1500 w_p: 1500	s_{tot}: 250–350 s_2: 100–200	170	–	Multilayer system
Altafim et al. (2009)	(c)	s_1: 50	w_a: 1500 w_p: 1500	s_{tot}: 200 s_2: 100	160	–	
Basso et al. (2007)	(c)	s_1: 50–75	-	s_{tot}: 160	13	–	Difficult production process
Zhang et al. (2006)	(d)	s_1: 12.5	w_a: 1000 w_p: 200	s_{tot}: 50–180 s_2: 15–105	1300	–	Multilayer system with air voids of 15 µm
Hu and Von Seggern (2006)	(e)	s_1: 12.5	–	s_{tot}: 88 s_2: 63	800	–	Fibrous ePTFE between FEP layers
Basso et al. (2006)	(c)	s_1: 50–75	w_a: 4000–8000 (round)	s_{tot}: 200–250 s_2: 100	–	–	Examination of a single cavity
Altafim et al. (2006)*	(c)	s_1: 50–75	w_a: 1000 (round)	–	500	–	Pressure applied through a vacuum
Altafim et al. (2005)	(c)	s_1: 50–75	w_a: 1000 (round)	–	500	–	Pressure applied through a vacuum
Altafim et al. (2003)	(c)	s_1: 80	–	s_{tot}: 240 s_2: 30	310	–	Aluminum-foil as back-electrode, Shellac as spacer

Letters for type refers to Fig. 1(c)–(f)

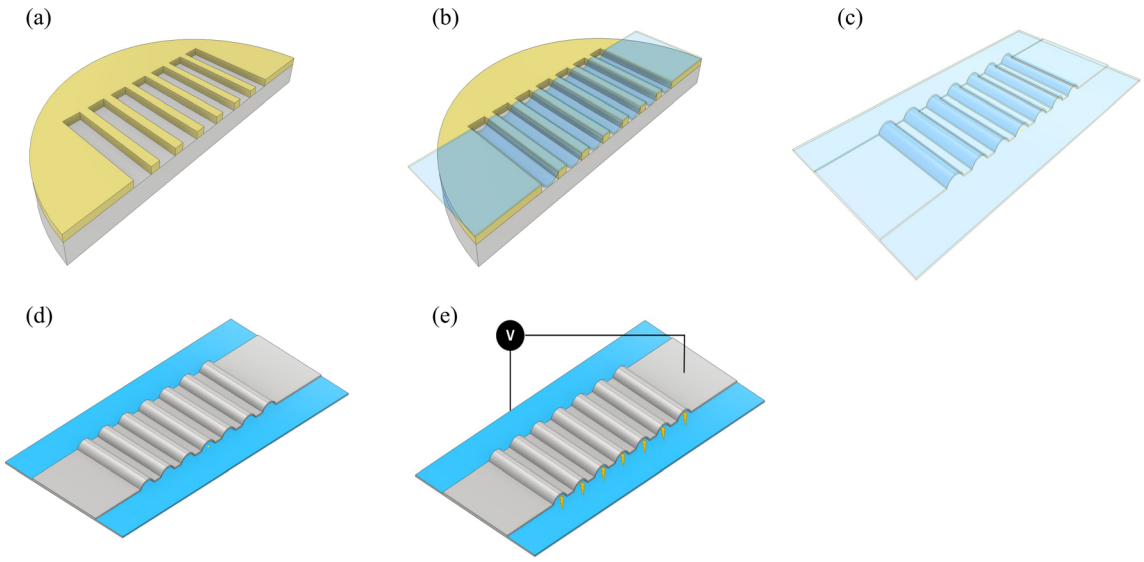

Fig. 2 Schematic of the production process of FEP piezoelectrets. After the preparation of a SU-8 template (**a**), the FEP-foil is thermoformed (**b**). By bonding two layers of FEP, the thermoformed materials form air cavities (**c**). After metallization of the stack (**d**), a charging process induces charges, stored at the interface between air and FEP (**e**)

Table 1 gives a comprehensive review of the literature on FEP-based piezoelectret research including relevant geometric, piezoelectric, and mechanical parameters. As numerous different approaches for the fabrication piezoelectrets have been developed, only the most important parameters influencing the performance are compared and concepts are classified into four main categories, see Fig. 1c–f. To increase the comparability of these studies, research concerning PTFE-based piezoelectrets is not considered in this review.

For the determination of Young's modulus usually dielectric resonance spectroscopy is applied, which is only valid for homogeneous samples. As some structures are not homogeneous in height, the calculated values should only be considered as approximation. Referenced values in Table 1 describe the best reported values of each publication. For the d_{33}-coefficient the highest, quasistatic value is listed, for Young's modulus the lowest value. If multiple structure sizes have been evaluated, there is one row for each experiment. Values marked with * are based on assumptions referring to previous publications. Geometrical parameters strongly influence the properties of the piezoelectric devices and their optimization has been a goal of all reviewed studies in Table 1.

As a quintessence of the literature review, one can draw some general conclusions: The overall piezoelectric activity increases with the reduction of the FEP-foil thickness, where thin FEP-foils result in a low Young's modulus, which consequently improves the mechanical properties. Furthermore, thin foils allow for a high charge density on the electrodes, as this value is directly proportional to layer thickness. To date the thinnest FEP-foil commercially available is 12.5 µm thick. Void-height is another crucial parameter as its miniaturization causes large capacitances and electrical fields. On the other hand, air damping increases with decreasing void sizes deteriorating the overall performance of the piezoelectric device. All discussed parameters are summarized in Table 3 in the appendix.

3 Fabrication process

3.1 Preparation of the thermoforming-templates

State-of-the-art thermoforming-templates for FEP - based piezoelectrets are processed by milling solid materials like copper or aluminum. For cost effective batch fabrication and good reproducibility alternative processing methods like the well-established MEMS-technology are desirable. A newly proposed fabrication process based on photolithographically structured thermoforming-templates is described in Table 2. Here, we propose the usage of the thick negative photoresist SU-8 100 (MicroChem, USA) to produce thermoforming-templates with horizontal structure sizes ranging from 1000 µm down to 300 µm and vertical structure sizes of 90 µm and below. The transparent photoresist offers high mechanical stability over a wide temperature range of up to 350 °C. For optical alignment of templates and foils, we use transparent glass wafers (Schott, Germany) as substrate. As adhesion between glass and SU-8 is a critical parameter for bonding and thermoforming, a careful treatment of the SU-8 during processing is necessary. It is well known that long soft-baking as well

Table 2 Processing parameters of SU-8 100 thermoforming-templates with a height of approx. 90 µm

Step	Description	Parameters
Pre-treatment	Sample cleaning	Nitrogen
	Dehydration	20 min @ 150 °C on a hotplate
	Spin-coating	TI-Prime 30 s @ 3000 rpm
	Bake	2 min @ 120 °C
1	Spin-coating SU8-100	15 s @ 1000 rpm, 30 s @3000 rpm
2	Softbake	20 min @ 65 °C, 60 min @ 95 °C-ramp with 3 °C/min, hood to slow down solvent evaporation, ramp down to RT with 3 °C/min
3	Illumination	UV Cube, 1200 mJ/cm^2@ 365 nm
4	Break	20 min for better processing
5	Post exposure bake	20 min @ 65 °C, 60 min @ 95 °C-ramp with 3 °C/min
6	Development	Mr 600 dev, 4 min with stirring, 1 min in fresh Mr 600 dev for better edges
7	Cleaning	Rinsing with isopropanol
		Dry blowing with nitrogen
8	Hardbake	60 min @ 150 °C on a hotplate

as long post-exposure-baking times with slow temperature ramps increase the thermal stability, which is the reason for long processing times in Step 2 and 5 of the production process.

Following the processing steps described in Table 2, thermoforming-templates with structure heights of approx. 90 µm and air void widths ranging from 1000 µm down to 300 µm were fabricated. The dimensions of the four sample types are:

- w_a = 1000 µm with a mean-height of s_2 = 93.5 µm,
- w_a = 500 µm with a mean-height of s_2 = 91.7 µm,
- w_a = 400 µm with a mean-height of s_2 = 86.9 µm,
- w_a = 300 µm with a mean-height of s_2 = 92.5 µm.

3.2 Thermoforming

For the thermoforming of a 12.5 µm thick FEP-foil (Lohmann, Germany) a hydraulic heat press (BluePRESSLine PNEU, Walter Schulze GmbH, Germany) was utilized. After placing the FEP on top of the thermoforming-template, a soft rubber pad was added to the stack, clamped into the hydraulic press, and heated at 120 °C for 10 min. Next, a mechanical pressure of 2 bar was applied for 10 min, during which the thermoforming process took place. Finally, the stack cooled slowly down to temperatures below 70 °C before pressure release prohibiting the back-forming of the foil. A graph of the process parameters as function of time is shown in Fig. 3.

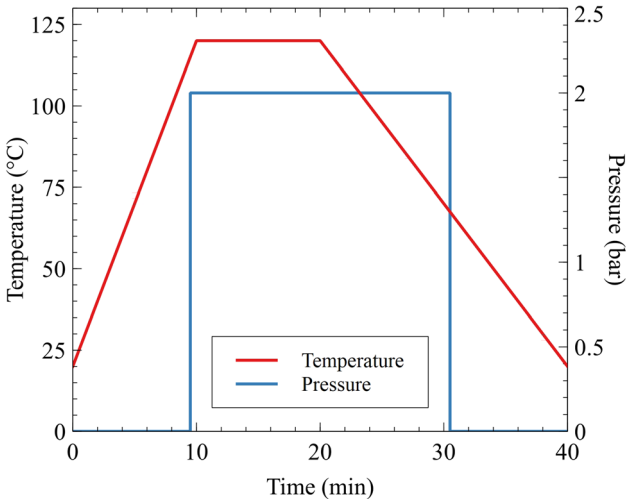

Fig. 3 Temperature and pressure during the thermoforming process

3.3 Assembly and charging of piezoelectrets

After thermoforming, the samples were metallized with 100 nm of chromium on the top side of the FEP (front electrode), also see Fig. 1b, where the chromium is a good trade-off between adhesion properties on FEP and electrical conductivity (Chang et al. 1990). The metallization was carried out with a sputtering process (300 W, 15 min) and a shadow-mask, resulting in an electrode area of 2×2 cm^2. Afterwards, samples were negatively corona charged to a surface potential of approximately –500 V (on the non-metallized surface) and the surface potentials was controlled with a non-contact electrostatic voltmeter (Trek

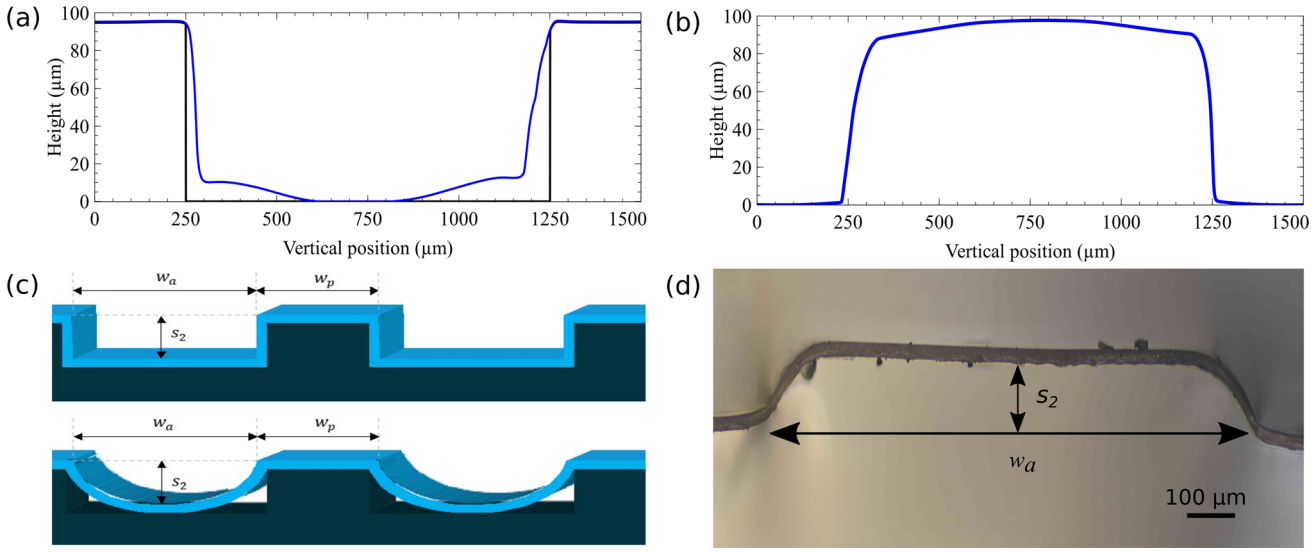

Fig. 4 Shape of thermoformed structures. **a** depicts a profilometer measurement of a thermoformed FEP-foil (blue line) inside of the thermoforming template (black line), while **b** shows the same foil released from the template. These measurements indicate a box-shaped profile after thermoforming. **c** Two analytically describable cases are a box-shaped and a catenary profile. **d** shows cross-section micrograph of a thermoformed FEP-foil with w_a= 1000 µm. The form can be approximated by a box-shaped profile

541-1, Trek Inc., New York, USA). As back electrode, a four inch glass wafer, metallized with a 150 nm thick chromium layer was used. For mounting, the charged foil was carefully adjusted onto the back electrode. Through electrostatic attraction, the foil adheres to the back electrode. Following this procedure, unipolar piezoelectrets, charged to a surface potential of –500 V, have been manufactured. A schematic cross-section of these unipolar piezoelectrets is depicted in Fig. 1b.

3.4 Measurement set-ups

To analyze the results of the fabrication process, profilometer measurements and microscopic analysis of the thermoformed foils have been conducted. The profilometer DEKTAK XT (Bruker, Germany) was used, equipped with a standard tip with an opening angle of 45° and a tip apex of 12.5 µm. To avoid modification of the soft FEP-foil during measurements, the force of the tip was adjusted to 0.1 mN, which is too low to indent the thermoformed structures.

For electrical characterization of the samples, static capacitance and charge sensitivity measurements at different frequencies were employed. For static capacitance measurements, different seismic masses were attached to the samples and capacitance was measured with a LCR-meter at a measurement frequency of 1 kHz. For charge sensitivity measurements, the setup consisted of a modal shaker Smartshaker K2007E01 (The Modal Shop, USA) with a Spider 81-B vibration controller with integrated charge amplifier (Crystal Instruments, USA) and an in-axis acceleration sensor (PCB Piezotronics, USA). Measurements were carried out two hours after charging. During measurement, the shaker excites the sample with added seismic masses at a constant acceleration over a defined frequency band. To get a uniform contact surface between the seismic mass and the foils we glued a 2×2 cm^2 glass plate with a weight of 1 g to the seismic mass. This weight was taken into account in the measurements. Because of undesirable, large displacements at low frequencies, excitatory frequencies were limited to values larger than 50 Hz. The charge generated by the piezoelectret was measured at its maximum, and taken to calculate the root-mean-square (RMS) value. With this setup, it is possible to measure the charge sensitivity at an acceleration of 1 × g in the range of 50–1000 Hz with different seismic masses.

4 Results

4.1 Thermoformed structures

To evaluate the accuracy of the thermoforming process, described in Sect. 3.2, thermoformed FEP-foils were measured with a profilometer inside the thermoforming-template, see Figure 4a, and after being released from the template, see Fig. 4b. Exemplary, this is depicted in Fig. 4a, where the black line illustrates the profile of the template with a structure width of 1000 µm and height of 93.5 µm. The blue line represents the thermoformed foil. In Fig. 4b the FEP-foils is measured in its released form (upside down). For all sample geometries, we find that the

horizontal structure widths w_a is reproducible within ± 5 µm as compared to the template dimensions, see Fig. 4b. The vertical height s_2 of the released structure exceeds in the center of the air void the height of the template by approximately 3 % due to expansion, while edges of the structure do not exactly represent the template. Assuming two analytically describable cases, namely box-shaped or catenary profile, we consider the thermoformed structure rather box-shaped than catenary as it has distinct edges, see Fig. 4c. This assumption is used later for the calculation of the static capacitance, see Table 4 in the appendix. In addition, optical micrographs on cross-sections were made to achieve more information on the foil's profile. These results as well reveal a cross-section more similar to a box-shape than to a catenary profile, see Fig. 4d. The foil thickness s_1 is 12.5 µm. This is the thinnest FEP-foil commercially available. As we stated earlier in Sect. 2, thin FEP-foils are beneficial for the performance of piezoelectrets.

4.2 Charge sensitivity and deformation of voids

The charge sensitivity Q_{Sens} is measured for assembled and charged samples with varied void width w_a and for varied seismic masses at an acceleration of 1 x g. The results are depict in Figs. 5 and 7, respectively.

For all samples, charge sensitivity is a function of frequency and shows distinct characteristics. For low frequencies, we observe a relatively high and constant charge sensitivity. At frequencies between 150 and 300 Hz all samples show a clear resonance for Q_{Sens}, depending on voids' width w_a and seismic mass. For frequencies above the resonance, Q_{Sens} decays fast with approximately 40 dB/decade.

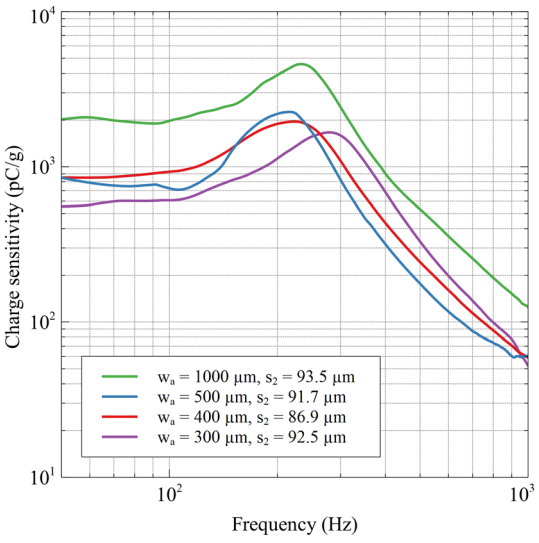

Fig. 5 Measured charge sensitivity with varied void width w_a at an acceleration of 1 × and a seismic mass of 21 g. All curves have been smoothed

In Fig. 5, samples with large void width w_a (void height s_2 is for all samples more or less the same) show highest charge sensitivity, which can be explained with the mechanical softest of the large air voids. With decreasing width w_a the stiffness of the system increases, resulting in reduced sensitivities as well as higher resonant frequencies. Note, that the sample with w_a = 1000 µm seems to be an outliner from this rule as the resonance frequency is higher than expected. To investigate this behaviour, the cross-section of the voids under the load of seismic masses are depicted in Fig. 6. One can observe an increasing deformation of the thermoformed FEP-foil under mechanical load for masses of 21 g and above. The original void structure deforms into into two smaller cavities, which is a possible explanation for the higher stiffness and thus higher resonant frequency. Interestingly, these deformations have not been observed for voids with a width of w_a = 500 µm and below (results not shown).

As their charge sensitivity is most promising, samples with large void width w_a= 1,000 µm (s_2 = 91.6 µm) are examined in more detail. Seismic masses ranging from 6 to 101 gram are applied at an acceleration of 1 × g, with results are depicted in Fig. 7. As expected, for decreasing seismic masses the resonance is shifted to high frequencies and charge sensitivity decreases. With a seismic mass of 21 g, we achieved a charge sensitivity Q_{Sens} of 5461 pC/g in resonance. This corresponds to a piezoelectric d_{33}-coefficent of 26,508 pC/N, using the equation $d_{33} = \frac{Q_{sens}}{m}$. With a seismic mass of 101 gram (and thus a deformed foil), we achieved a Q_{Sens} of 15,354 pC/g. This corresponds to a piezoelectric d_{33}-coefficent of 15,497 pC/N. Such a nonlinearity of d_{33}-coefficient is often observed in piezoelectrets (Zhang et al. 2015).

4.3 Application as energy-harvester

The output-power $P_{opt}(m)$ of the piezoelectret is calculated for an acceleration of 1 × g with the charge $Q = Q_{Sens}$ x g (see Eq. 1). For maximal power generation, it is necessary to match the electrical impedance of the load with that of the piezoelectret. The matching load $R_{opt}(m)$ is calculated at the resonant frequency $f_0(m)$ where admittances compensate each other, with both parameters ($R_{opt}(m)$, $f_0(m)$) being a function of the applied seismic mass m (see Eq. 2). The static capacitance $C_{stat}(m)$ is measured for different seismic masses (see Table 4 in the appendix).

$$P_{opt}(m) = \frac{1}{2} \cdot R_{opt}(m) \cdot \omega^2 \cdot Q(m)^2 \quad (1)$$

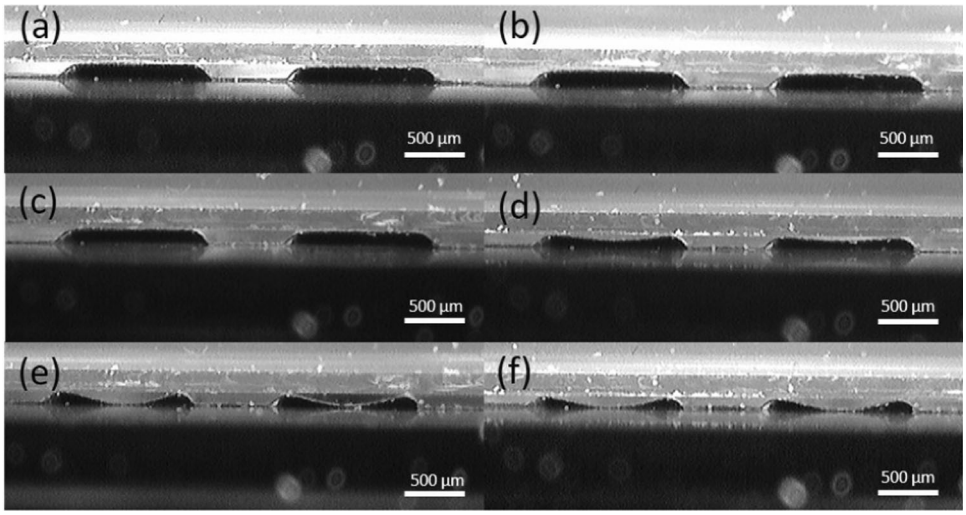

Fig. 6 Cross-section micrograph of a single cavity under the effect of a seismic mass. With higher masses, the single cavity tends to form two cavities. The force was added on a 2×2 cm^2 sample, and increased as follows: **a** 1 g, **b** 6 g, **c** 11 g, **d** 21 g, **e** 51 g, and **f** 101 g

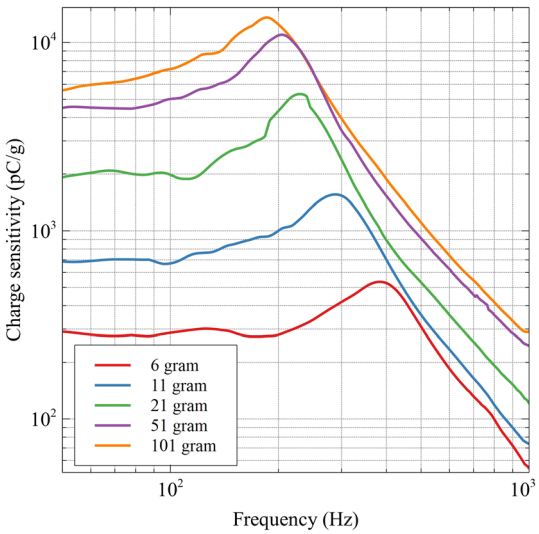

Fig. 7 Measured charge sensitivity for different seismic masses on a structure with w_a = 1000 µm, s_2 = 91.6 µm and a sample size of 2×2 cm^2. The acceleration in all measurements was 1 × g. All curves have been smoothed

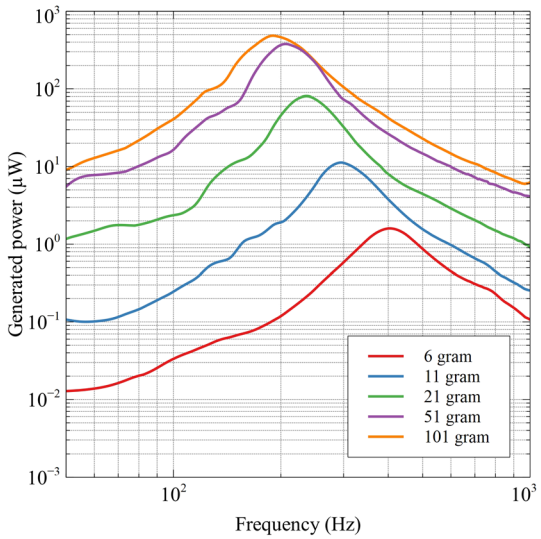

Fig. 8 Calculated output-power over an optimized load resistor for a sample with w_a = 1000 µm, s_2 = 91.6 µm and a sample size of 2×2 cm^2. All curves have been smoothed

with

ω: Vibration angular frequency [ω] = 1/s Q: Charge [Q] = C

$$R_{opt}(m) = \frac{1}{2 \cdot \pi \cdot f_0(m) \cdot C_{stat}(m)} \quad (2)$$

In Fig. 8, the calculated output-power for the sample with w_a = 1000 µm and s_2 = 91.6 µm is presented for different seismic masses. Like the charge sensitivity, the output-power strongly depends on the excitatory frequency and reaches a maximum at distinct values depending on the seismic mass. A fact that is of high interest for applications, as mechanical matching is required for maximal output.

Best values are achieved for a seismic mass of 101 gram at resonance of 170 Hz. Here, the output-power reaches a maximum at 0.51 mW. As expected, the output-power decreases fast with smaller seismic masses. At a value of 51 gram, the output-power is down to 0.41 mW and decreases rapidly for smaller masses, so that with a seismic mass of 6 gram only 2 µW are generated. One can analytically derive, that the generated power is proportional to $m^{3/2}$ (see Ma et al. (2019)). In Fig. 9 the maximum generated power values (calculated from measured values) are depicted as a function of seismic mass. For masses between 1 and 51 g, measurements show good agreement with the analytical model. However, for the seismic mass of 101 g the generated power is well below expectation, which may

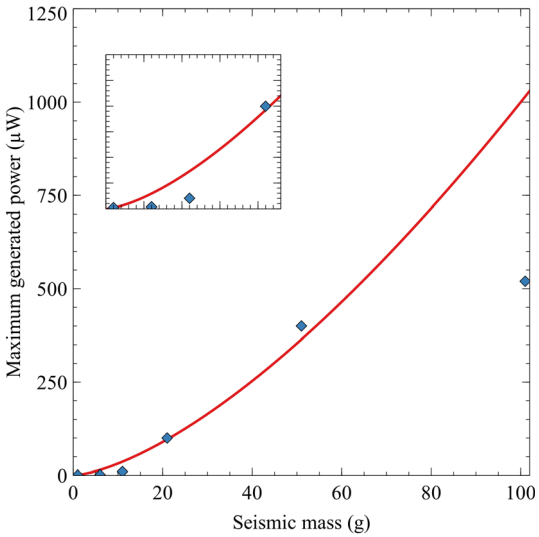

Fig. 9 Calculated output-power for optimized load resistor (sample dimensions w_a = 1000 µm and s_2 = 91.6 µm). Markers represent the values calculated from measured capacitance and charge sensitivity according to Fig. 8, the line describes the analytical model proportional to $m^{3/2}$

be explained with a large deformation of the void shape with a tendency to form two cavities (see Fig. 6 f).

To proof the usability of the new piezoelectrets for applications, we performed a test with a light emitting diode (LED) between front and back electrode. These LEDs have a typical power rating of a few milliwatt. Distinct lighting was visible at the resonant frequency of 170 Hz for an acceleration of only 0.5 × g, which is comparable to accelerations and frequency of typical home application such as blenders, ventilating fans or microwave oven (Ab Rahman and Kok 2001).

5 Conclusion

To achieve widespread usage of piezoelectrets as energy harvester or mechanical sensor, their potential must be fully exploited. Therefore, an optimization of their output power or sensitivity (depending on the scope of application) and of the fabrication process is crucial. In this work we present a comprehensive overview of most recent progress in the field of polymer piezoelectrets with a focus on the polymer FEP. A wide variety of designs is presented and best results are tabulated.

In the second part of the paper, a new photolithography-based fabrication process for unipolar, FEP-based piezoelectrets is presented. We demonstrate, that this process facilitates the fabrication of thermoforming templates with highly controllable vertical and horizontal structure sizes allowing for devices with tailored properties. The approach is favorable for rapid prototyping and the adaption of design parameters to specific use cases. The automation of the assembly process was not addressed in this work and will be the focus for future work as it may pave the way to high-throughput processing.

The air void shapes of the fabricated piezoelectrets, which determine the overall mechanical behavior, were analyzed thoroughly and it is shown that the thermoformed micro-structures are fabricated with good dimensional accuracy. To examine the influence of lateral miniaturization in unipolar FEP-based piezoelectrets, vertical structure size was varied, while the air gap height was kept at about 90 µm. Piezoelectrets were fabricated with a thin (12.5 µm) FEP-foil and charge sensitivity as well as power generation has been exploited.

As already described in literature, we found that large void sizes are favorable for the overall performance of the piezoelectret due to low air damping. Accordingly, we achieved the highest piezoelectric d_{33}-coefficient of 26,508 pC/N in resonance for a large void width of w_a = 1000 µm and a seismic mass of 21 g. Further increasing of the width however seems not target-oriented, as we see that the mechanically soft structures deform easily when a load is applied. In deed, we found that for seismic masses larger than 21 gram clear deformations are induced in the thin FEP-foil with the tendency to form two smaller voids. We believe that this is the reason for the decline of d_{33} with load. Furthermore, this deformations are also a limiting factor for power generation which increases with load. Measured values for large seismic masses are well below theoretical values expected from the analytical model (of the original). The best power generation we achieved for a seismic mass of 101 g was 0.51 mW at an acceleration of 1 × g for an area of 2×2 cm^2 whereas a theoretical value of approximately 1 mW was expected.

Appendix A

See Tables 3 and 4.

Table 3 Parameters influencing an optimized piezoelectric behavior of FEP-based piezoelectrets

Origin	Parameter	Target	Influence of miniaturization	Limitation
Mechanical	Y	Minimizing	Smaller air voids increase Young's modulus through air-damping.	Increasing Young's modulus is a side effect of miniaturization.
Electrical	σ_{rem}^{max}	Maximizing	Smaller air voids result in less remnant charge, as back discharges occur faster at smaller distances. However, as a result of Paschen's law, for very small air voids the remnant charge should increase.	The validity of the Paschen's law is only proven down to 8 µm (Babrauskas 2013). It is not clear if smaller air voids will further increase σ_{rem}^{max}.
Electrical	ϵ_r	Maximizing	No influence.	The dielectric constant of FEP is 2.1.
Mechanical and electrical	s_1	Minimizing	Thinner solid layers result in smaller Young's modulus. Hence s_1 should be as thin as possible.	To date the thinnest FEP commercially available is 12.5 µm.
Mechanical and electrical	s_2	Minimizing	The air void thickness should be minimized to increase the change in induced charge.	Too small air voids are difficult to produce and can induce back discharges.

Table 4 Calculated values of the capacitance of thermoformed FEP-foils for box-shaped and catenary profiles for an area of 2×2 cm^2 without an applied seismic mass

	s_2 = 93.5 µm		s_2 = 91.7 µm		s_2 = 86.8 µm		s_2 = 92.5 µm	
	w_a = 1000 µm		w_a = 500 µm		w_a = 400 µm		w_a = 300 µm	
	w_p = 500 µm		w_p = 250 µm		w_p = 200 µm		w_p = 150 µm	
	Capacitance							
	in pF/cm^2	in pF	in pF/cm^2	in pF	in pF/cm^2	in pF	in pF/cm^2	in pF
Box-shaped	61.28	245.11	61.48	245.92	62.05	248.22	61.39	245.56
Catenary	71.12	284.48	71.22	284.90	71.93	287.72	70.77	283.07
Measured	55	220.00	30.70	122.80	39.15	156.60	42.97	171.90

Acknowledgements The authors gratefully acknowledge financial support from the Zentrum für Wisschenschaftliche Services und Transfer (ZeWiS) and the Bundesministerium für Bildung und Forschung in the frame of FHprofUnt2015 (HARVIS 03FH003PX5). Furthermore, the authors want to thank Prof. G. Sessler for helpful discussion on the characterization and Prof. H. von Seggern as well as Dr. S. Zhukov for the help and the possibility to perform the corona charging.

Funding Open Access funding enabled and organized by Projekt DEAL.

References

Ab Rahman MFB, Kok SL (2011) Investigation of useful ambient vibration sources for the application of energy harvesting. In: IEEE Stud. Conf. Res. Dev, IEEE, pp 391–396

Altafim R, Dias C, Neto LG et al (2003) Piezoelectricity of multilayers space-charge electrets from teflon fep film with homogeneous voids distributed on its surface. In: Annu. Rep.—Conf. Electr. Insul. Dielectr. Phenom, IEEE, pp 225–228

Altafim R, Basso H, Neto LG et al (2005) Piezoelectricity in multi-air voids electrets. In: Annu. Rep.—Conf. Electr. Insul. Dielectr. Phenom, IEEE, pp 669–672

Altafim R, Basso HC, Altafim R et al (2006) Piezoelectrets from thermo-formed bubble structures of fluoropolymer-electret films. IEEE Trans Dielectr Electr Insul 13(5):979–985

Altafim RAP, Qiu X, Wirges W et al (2009) Template-based fluoroethylenepropylene piezoelectrets with tubular channels for transducer applications. J Appl Phys 106(1):014106

Altafim R, Qiu X, Wirges W et al (2010) Template-based fluoropolymer ferroelectrets with multiple layers of tubular channels. In: Annu. Rep.—Conf. Electr. Insul. Dielectr. Phenom, IEEE, pp 1–4

Altafim R, Altafim R, Basso H et al (2011a) Fluoroethylenepropylene ferroelectrets with superimposed multi-layer tubular void channels. In: Annu. Rep.—Conf. Electr. Insul. Dielectr. Phenom, IEEE, pp 133–136

Altafim R, Basso H, Altafim R et al (2011b) A comparison of polymer piezoelectrets with open and closed tubular channels: pressure dependence, resonance frequency, and behavior under humidity. In: 14th Int. Symp. Electrets, IEEE, pp 213–214

Altafim RAP, Rychkov D, Wirges W et al (2012a) Laminated tubular-channel ferroelectret systems from low-density polyethylene films and from fluoroethylene-propylene copolymer films-a comparison. IEEE Trans Dielectr Electr Insul 19(4):1116–1123

Altafim RAP, Altafim RAC, Qiu X et al (2012b) Fluoropolymer piezoelectrets with tubular channels: resonance behavior controlled by channel geometry. Appl Phys A 107(4):965–970

Araújo EBL, de Amorim MF, Altafim RAP et al (2015) Thin teflon-fep capacitors with open-tubular channels employed on low-pressure measurements for smart-grid monitoring systems. In: 2015 IEEE Conf. Electr. Insul. Dielectr. Phenom. (CEIDP), IEEE, pp 311–313

Assagra YAO, Altafim RAC, Altafim RAP (2015) Thermo-formed piezoelectrets with open-tubular channels produced from water-filled fep pads. In: 2015 IEEE Conf. Electr. Insul. Dielectr. Phenom. (CEIDP), IEEE, pp 648–651

Babrauskas V (2013) Arc breakdown in air over very small gap distances. In: Conference: Interflam, pp 1489–1498

Basso HC, Aquino C, Altafim R et al (2006) Piezoelectricity of a single bubble formed by two oppositely charged teflon®-fep films. In: Annu. Rep.—Conf. Electr. Insul. Dielectr. Phenom, IEEE, pp 146–149

Basso HC, Altafim R, Altafim R et al (2007) Three-layer ferroelectrets from perforated teflon®-ptfe films fused between two homogeneous teflon®-fep films. In: Annu. Rep.—Conf. Electr. Insul. Dielectr. Phenom, IEEE, pp 453–456

Cao G, Zhang XQ, Sun Z et al (2011) Polarization and properties of laminated fluoropolymer films. Mater. Trans Tech Publ, Sci. Forum, pp 359–365

Chang CA, Kim YK, Schrott A (1990) Adhesion studies of metals on fluorocarbon polymer films. J Vac Sci Technol A 8(4):3304–3309

Emmerich F, Thielemann C (2018) Optimizing dimensions of unipolar Teflon-FEP piezoelectrets with micro-system-technology. In: Conf Ser, J Phys

Falconi D, Altafim R, Altafim R et al (2011) Multi-layers fluoroethylenepropylene (FEP) films bounded with adhesive tape to create piezoelectrets with controlled cavities. In: 2011 Annu. Rep.—Conf. Electr. Insul. Dielectr. Phenom. (CEIDP), IEEE, pp 137–140

Fang P, Holländer L, Wirges W et al (2012) Piezoelectric d33 coefficients in foamed and layered polymer piezoelectrets from dynamic mechano-electrical experiments, electro-mechanical resonance spectroscopy and acoustic-transducer measurements. Meas Sci Technol 23(3):035604

Gerard M, Bowen CR, Osman FH (2011) Processing and properties of PTFE-FEP-PTFE ferroelectret films. Ferroelectrics 422(1):59–64

Hillenbrand J, Pondrom P, Sessler G (2015) Electret transducer for vibration-based energy harvesting. Appl Phys Lett 106(18):183902

Hu Z, Von Seggern H (2006) Breakdown-induced polarization buildup in porous fluoropolymer sandwiches: a thermally stable piezoelectret. J App Phys 99(2):024102

Lekkala J, Poramo R, Nyholm K et al (1996) EMF force sensor—a flexible and sensitive electret film for physiological applications. Med Biol Eng Comput 34:67–68

Lou KX, Zhang X, Xia Z (2012) Piezoelectric performance of fluor polymer sandwiches with different void structures. Appl Phys A 107(3):613–620

Ma X, Zhang X, Sessler GM et al (2019) Energy harvesters based on fluorinated ethylene propylene unipolar ferroelectrets with negative charges. AIP Adv 9(12):125334

Ma X, Yang X, von Seggern H et al (2021) Tuneable resonance frequency vibrational energy harvester with electret-embedded variable capacitor. IET Nanodielectr 4(2):53–62

Medeiros L, Basso H, Altafim R et al (2012) Multi-layer piezoelectret hydrophone for ultrasonic applications. In: 2012 IEEE Int. Ultrason. Symp, IEEE, pp 1–4

Nepal N, Altafim RAP, Mellinger A (2017) Space charge deposition in tubular channel ferroelectrets: a combined fluorescence imaging/LIMM study with finite element analysis. J Appl Phys 121(24):244103

Qiu X, Gerhard R (2016) Influence of the ambient gas on the charging efficiency of tubular-channel fluoroethylenepropylene (FEP) copolymer ferroelectrets. In: 2016 IEEE Conf. Electr. Insul. Dielectr. Phenom. (CEIDP), IEEE, pp 85–88

Rychkov D, Altafim RAP, Gerhard R (2014) Unipolar ferroelectrets-following the example of the electret microphone more closely. In: 2014 IEEE Conf. Electr. Insul. Dielectr. Phenom. (CEIDP), IEEE, pp 860–862

Rychkov D, Wirges W, Gerhard R et al (2015) Unipolar Teflon®-FEP ferroelectrets-choice of negative electret charge enhances stability. In: 2015 IEEE Conf. Electr. Insul. Dielectr. Phenom. (CEIDP), IEEE, pp 84–86

Sun ZL, Zhang XQ, Cao GX et al (2011a) Performance of piezoelectrets made of non-porous polytetrafluoroethylene and fluoroethylenepropylene layers. In: Mater. Trans Tech Publ, Sci. Forum, pp 343–347

Sun Z, Zhang X, Xia Z et al (2011b) Polarization and piezoelectricity in polymer films with artificial void structure. Appl Phys A 105(1):197

Wang Y, Wu L, Zhang X (2015) Energy harvesting from vibration using flexible floroethylenepropylene piezoelectret films with cross-tunnel structure. IEEE Trans Dielectr Electr Insul 22(3):1349–1354

Wirges W, Raabe S, Qiu X (2012) Dielectric elastomer and ferroelectret films combined in a single device: how do they reinforce each other? Appl Phys A 107(3):583–588

Zhang X, Hillenbrand J, Sessler GM (2006) Thermally stable fluorocarbon ferroelectrets with high piezoelectric coefficient. Appl Phys A: Mater Sci Process 84(1–2):139–142

Zhang X, Cao G, Sun Z et al (2010) Fabrication of fluoropolymer piezoelectrets by using rigid template: structure and thermal stability. J Appl Phys 108(6):064113

Zhang X, Hillenbrand J, Sessler G et al (2012) Fluoroethylenepropylene ferroelectrets with patterned microstructure and high, thermally stable piezoelectricity. Appl Phys A 107(3):621–629

Zhang X, Zhang X, Sessler GM et al (2013) Quasi-static and dynamic piezoelectric responses of layered polytetrafluoroethylene ferroelectrets. J Phys D: Appl Phys 47(1):015501

Zhang X, Sessler GM, Wang Y (2014) Fluoroethylenepropylene ferroelectret films with cross-tunnel structure for piezoelectric transducers and micro energy harvesters. J Appl Phys 116(7):074109

Zhang X, Wu L, Sessler GM (2015) Energy scavenging from vibration with two-layer laminated fluoroethylenepropylene piezoelectret films. In: 2015 Jt. IEEE Int. Symp. Appl. Ferroelectr. (ISAF), Int. Symp. Int. Funct. (ISIF), and Piezoelectric Force Microscopy Workshop (PFM), IEEE, pp 24–27

Zhang X, Pondrom P, Wu L et al (2016a) Vibration-based energy harvesting with piezoelectrets having high d 31 activity. Appl Phys Lett 108(19):193903

Zhang X, Sessler GM, Xue Y et al (2016b) Audio and ultrasonic responses of laminated fluoroethylenepropylene and porous

polytetrafluoroethylene films with different charge distributions. J Phys D: Appl Phys 49(20):205502

Zhang X, Sessler GM, Ma X et al (2018) Broad bandwidth vibration energy harvester based on thermally stable wavy fluorinated ethylene propylene electret films with negative charges. J Micromech Microeng 28(6):065012

Zhukov S, Eder-Goy D, Biethan C et al (2017) Tubular fluoropolymer arrays with high piezoelectric response. Smart Mater Struct 27(1):015010

Zhukov S, von Seggern H, Zhang X et al (2020) Microenergy harvesters based on fluorinated ethylene propylene piezotubes. Adv Eng Mater 12:1901399

Zuo X, Chen L, Pan W et al (2020) Fluorinated polyethylene propylene ferroelectrets with an air-filled concentric tunnel structure: preparation, characterization, and application in energy harvesting. Micromachines 11(12):1072